Particle dynamics in magnetorheological suspensions using diffusing-wave spectroscopy

Eric M. Furst and Alice P. Gast*
Department of Chemical Engineering, Stanford University, Stanford, California 94305-5025
(Received 12 May 1998)

Magnetorheological suspensions acquire dipole moments in an external magnetic field. Suspensions of these dipolar particles rapidly aggregate to form long chains. We use diffusing-wave spectroscopy (DWS) and density-matched superparamagnetic emulsion droplets to probe the short-wavelength motion of the chains. The measured particle displacements are independent of the magnitude of the dipolar interactions at short times, but characterized by a constrained, subdiffusive motion at long times that slows as the dipolar interactions are increased. Our observations show good qualitative agreement with Brownian dynamics simulations of dipolar chains. [S1063-651X(98)08509-2]

PACS number(s): 83.80.Gv, 83.20.Jp, 82.70.Dd

I. INTRODUCTION

The unique field-induced rheological response of magnetorheological (MR) fluids has made them the focus of considerable attention in the past decade [1–6]. MR fluids are colloidal suspensions of paramagnetic particles in a nonmagnetic fluid. These fluids, along with their electrical analogs, electrorheological (ER) fluids, have been proposed as controllable fluids that are ideal for interfacing electronic controls with mechanical systems, such as dampers, clutches, and brakes [7,8]. When exposed to an external magnetic field, the particles in a MR suspension acquire dipole moments and aggregate to form chains in the field direction. The fluid structure depends on the volume fraction; dilute suspensions form weakly interacting single-particle chains, while when more concentrated, the particle chains cross-link laterally into a dense network. The latter structure is responsible for the unique rheological properties of MR suspensions: the quick formation of a network in response to an external field creates a rapid liquid-to-solid transition. Aside from their practical applications, MR suspensions are of fundamental interest because they allow us to probe the structure and dynamics of a suspension of particles interacting via a ''tunable'' anisotropic interaction. For instance, Zhan and co-workers recently applied paramagnetic colloids to study the effects of collective hydrodynamics on particle self-diffusion, taking advantage of the ability to vary and factor out direct particle interactions [9].

Recently, we have studied microscopic properties, such as the kinetics of chain growth and low-energy structures [10–12]. The suspension dynamics [13,14] are of interest since it has been proposed that Landau-Peierls thermal fluctuations of dipolar chains could be responsible for long-range attractions between chains [15]. Rigid dipolar chains produce a transverse magnetic field that decreases approximately as $\exp(-\rho/a)$ where ρ is the distance from the chain and a is the dipolar particle radius. Thus, chains separated by a distance greater than one diameter should interact weakly. In contrast, taking into account thermal fluctuations produces a mean-squared field that decreases as a power law: $\sqrt{\langle H^2 \rangle} \sim \sqrt{kTa}/\rho^2$. Thus, fluctuations may be responsible for the long-range lateral interactions in dipolar chains that greatly affect their response and final structures.

Here we report our initial studies of the dynamics of MR fluid suspensions using diffusing-wave spectroscopy (DWS). Our work utilizes particles that are density matched to the suspending solvent to minimize sedimentation. Previous work examining the fluctuations of dipolar chains used paramagnetic polystyrene beads which were at rest on a glass slide [14]. The use of a density-matched system and light scattering allows us to probe the dynamics of long chains fluctuating fully in three dimensions, free of interfacial interactions or hydrodynamic effects. Additionally, our application of DWS to study the dynamics of MR suspensions allows us to probe smaller length and time scales previously inaccessible through single scattering experiments or microscopic observation. Previous work by Ginder used similar methods to examine particle dynamics and structure formation in ER suspensions [16]. Here the DWS experiments were used to resolve the oscillatory electrophoretic motion of particles in an applied ac field along with an effective increase in the diffusivity due to a concentrated network formation; his aim was not to study the fluctuation spectrum of dipolar chains. Also, a thorough understanding of particle interactions in ER suspensions differs from that in MR suspensions due to the effects of surface charge, adsorbed water, and field inhomogeneities.

II. EXPERIMENT

We synthesized MR emulsion droplets following a method due to Bibette [17]. A ferrofluid (Rhône-Poulenc), composed of monodomain iron oxide particles suspended in octane, is emulsified into water using sodium dodecyl sulfate, SDS (Sigma, cmc=2.351 g/ml). The rough emulsion is fractionated by seven successive depletion aggregations with SDS micelles. We vary the particle density by manipulating the amount of octane in the ferrofluid; the particles in this study have a density of approximately 1.1 g/ml. We resuspend the particles in a D_2O-SDS solution ($\rho=1.10$ g/ml) at the SDS cmc to minimize sedimentation effects in our light scattering experiments. In this study we use particles of approximately 240 nm diameter, at a volume fraction, ϕ of

*Author to whom correspondence should be addressed.

0.005 and a magnetic susceptibility χ of 1.2.

When placed in an external magnetic field, the particles interact via an anisotropic dipolar potential

$$U(r,\theta)=\left(\frac{4\pi\mu^2}{\mu_0}\right)\frac{1-3\cos^2(\theta)}{r^3}, \tag{2.1}$$

where θ is the angle the particle centers form with the field direction, r is the distance between particle centers, and $\mu=\frac{4}{3}\pi a^3\mu_0\chi H$ is the induced dipole for a particle of radius a in a field of magnitude H. We characterize the dipole strength with [18]

$$\lambda=\frac{-U_{\max}}{kT}=\frac{\pi\mu_0 a^3\chi^2H^2}{9kT}. \tag{2.2}$$

Our experiments are conducted over a range of dipole strengths: $\lambda=4$, 7, 11, and 16.

The dynamics of our MR fluid are studied using a transmission geometry [19]. The MR fluid is placed in a spectrophotometer cuvette (Spectrocell) with a path length $L=10$ mm. The cuvette is centered in a uniform magnetic field generated by Helmholtz coils. Linearly polarized light from a 35 mW HeNe (Spectraphysics) at 632.8 nm is expanded to a plane wave with a 10× laser collimator and illuminates the face of the sample perpendicular to the field direction. The transmitted diffuse light is collected by two pinholes coupled to a multimode optical fiber. A cross-polarizer transmits only depolarized, highly multiply scattered light. The intensity fluctuations are measured using a photomultiplier (Thorn EMI) with a built-in amplifier-descriminator. We use a commercial correlator (Brookhaven Instruments, BI-9000AT) to calculate the intensity autocorrelation, $g^{(2)}(t)$. The electric field autocorrelation $g^{(1)}(t)$, is found using the Siegert relation, $g^{(2)}(t)=|g^{(1)}(t)|^2-1$.

When the magnetic field is applied, the dipolar particles rapidly aggregate to form chains. On longer time scales, the chains experience lateral interactions and coalesce to form thicker columns. We are interested in the fluctuation-induced lateral attraction causing this coalescence. Thus we developed an experimental protocol to produce conditions where the *fluctuations of individual chains* dominate the system dynamics. First, by minimizing the density difference between our droplets and the suspending fluid, we reduce the sedimentation-induced aggregation of chains. For our dynamic studies, the chains are first grown at $\lambda=16$ for 12 s, and then subjected to the desired field strength. This provides a consistent suspension structure as a starting point for measurements at each dipole strength, and avoids the initial ballistic motion of particles and small chains occurring when the field is first applied. Starting at 15 s, we collect autocorrelation data for 60 s. To assess the effect of the starting time, we repeat the experiments switching the field at 85 s and starting the autocorrelation at 90 s.

In the diffusion limit of light transport in turbid media, a photon executes a random walk with an average step length of l^*, characterizing the distance over which its direction is randomized. Since structure and interactions affect the value of l^* [19–22], we measure the diffuse transmittance of an expanded laser beam to monitor the change in light transport properties during an experiment. Changes in l^* are taken into account in our analysis. The initial value of l^* is found from by fitting the field-off data. The characteristic absorption length for photons diffusing in a medium having an absorption coefficient α is $l_a=\sqrt{l^*/3\alpha}$ [23,16]. This is found independently by varying the path length and measuring the diffuse transmittance through a sample without the magnetic field.

Light transport properties are also measured by removing the collimator and focusing the incident beam to a point source on the sample cuvette face. The transmitted diffuse light is collected on a charge-coupled device (CCD) array and recorded on videotape at a rate of 30 Hz. Images are captured from tape by averaging 20 video frames and processed to assess the evolution of anisotropic light transport in our samples after the field is applied and the magnetic chains begin growing.

III. RESULTS AND DISCUSSION

A. Effects of anisotropic light transport

In diffusing wave spectroscopy, the electric-field autocorrelation is a weighted sum:

$$g^{(1)}(\mathbf{r},t)=\int_0^\infty d\tau P(\mathbf{r},\tau)\exp[-(c/3l^*)k_0^2\langle\Delta r^2(t)\rangle\tau], \tag{3.1}$$

where $\langle\Delta r^2(t)\rangle$ is the mean-squared displacement of the scatterers and c is the speed of light in the medium. The probability $P(\mathbf{r},\tau)$ that a diffusing photon will arrive at position $\mathbf{r}$ and time τ is determined by solving the diffusion equation for the experimental geometry. The MR system is complicated by the fact that the suspension structure becomes anisotropic as the particles aggregate to form chains. In this case, the diffusion equation for the light energy density U is anisotropic:

$$\frac{\partial U(\mathbf{r},\tau)}{\partial\tau}=(D_\parallel\nabla_\parallel^2+D_\perp\nabla_\perp^2+1/\mu_a)U(\mathbf{r},\tau), \tag{3.2}$$

where μ_a is the characteristic time for photon absorption and $D_\parallel$ and $D_\perp$ are the light diffusion constants in the direction parallel and perpendicular to the orientation of the chains, respectively. The diffusive probability is found from $P(\mathbf{r},\tau)=U(\mathbf{r},\tau)/\int_0^\infty d\tau U(\mathbf{r},\tau)$. The anisotropic light diffusion problem may be reduced to the familiar isotropic form by rescaling the axes, such that for our geometry we have [24]

$$\left[\frac{\partial}{\partial\tau}-D\frac{\partial^2}{\partial\zeta^2}-\frac{1}{\mu_a}\right]U(\mathbf{r},\tau)=0, \tag{3.3}$$

where D is the average diffusivity and $\zeta=\sqrt{D/D_\perp}x$. This equation is valid as long as the plane-wave conditions are met experimentally; that is, both of the components of l^* parallel and orthogonal to the orientation of the scattering chains are much less than the width of our expanded beam. Equation (3.3) is solved using zero net-flux boundary conditions discussed elsewhere [19].

We note that Eq. (3.1) assumes the dynamic scattering cross section can be approximated with its form for a dilute

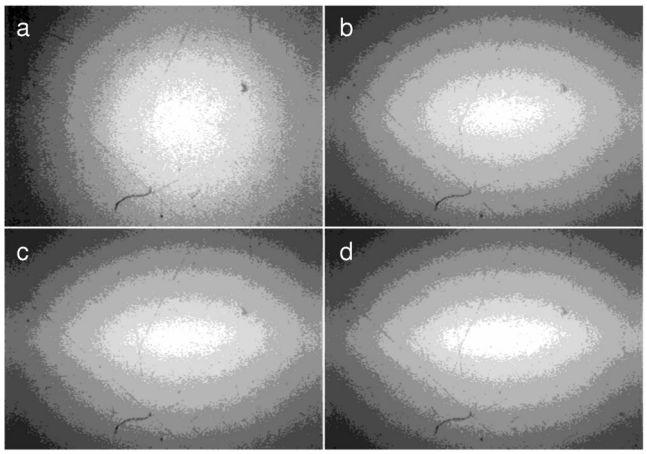

FIG. 1. Images showing depolarized diffuse intensity from a point source transmitted through a 10 mm sample with the field off and at $\lambda = 16$. The intensity is initially isotropic, but becomes anisotropic as chains form. The chains are oriented from top to bottom. Each image is 5.0 by 3.7 mm. (a) Field off. (b) Field on 45 s. (c) Field on 90 s. (d) Field on 150 s.

colloidal suspension [25]. Recently, an anisotropic multiple light scattering formalism has been developed and applied to light scattering in nematic liquid crystals [26–29]; however, the nature of light scattering in nematics differs from that in colloidal systems. For instance, the static structure factor in nematics diverges at low scattering angle q, and results in a vanishing scattering mean free path l_s while maintaining a finite l^* [30].

The magnitude of the light transport anisotropy is established through the steady-state transmission of a point-source through the sample. Figure 1 shows images of the diffuse depolarized intensity collected by our CCD camera for 45 and 150 s after the field is applied at $\lambda = 16$. The ratio of the major and minor axes increases rapidly to 1.6 at 15 s as the chains are initially formed. At 45 s, the ratio is 1.8 and increases slowly to 2.2 at 150 s; this small anisotropy validates the use of Eq. (3.3) with the scaled distance ζ. The ratios are insensitive to switching the field strength to lower values, and the images return immediately to the isotropic values when the field is turned off.

B. Estimation of l^* and l_a

The absorption length l_a is 1.12 ± 0.08 mm. Using this value and the calculated particle self-diffusion coefficient D_s, we fit the field-off autocorrelation to find $l^* = 790 \pm 10$ μm as shown in Fig. 3. The relatively large value of l^* compared with systems such as polystyrene spheres [20] can be attributed to the lower contrast of our droplets.

As mentioned previously, changes in the spatial arrangement and interactions of scatterers alter the diffuse transmittance through the sample. In the case of dense or interacting suspensions, l^* is proportional to the weighted average over the particle form factor $P(q)$ and structure factor $S(q)$ [19–22]:

$$l^{*-1} \propto 2k_0^{-2} \int_{4\pi} q^2 P(q) S(q) d\Omega. \tag{3.4}$$

To assess the effect of the dipolar interactions and chain

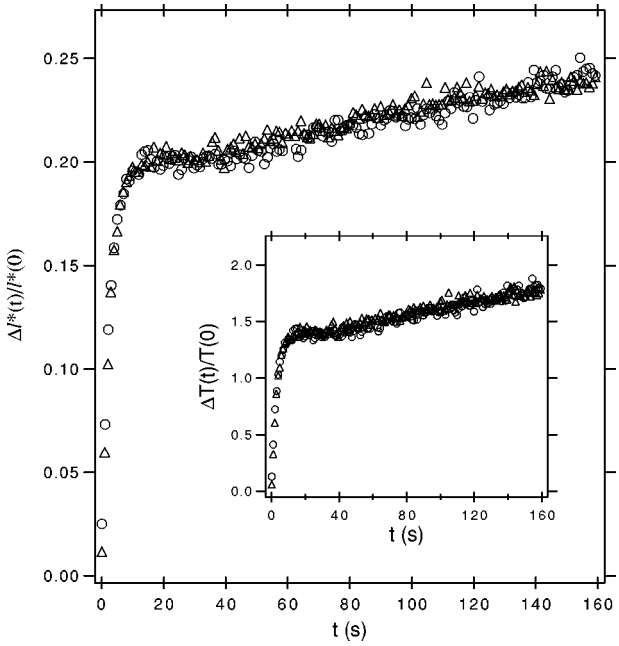

FIG. 2. The normalized change in l^* after the magnetic field is applied. Two data sets are shown: ($\triangle$) the field is held constant at $\lambda = 16$. ($\bigcirc$) The field is stepped to $\lambda = 7$ at 85 s. The inset shows the normalized change in transmittance used to calculate $\Delta l^*(t)/l^*(0)$.

structures on *the orientationally averaged value of the transport mean free path* l^*, we monitor the diffuse transmittance through our sample and measure the normalized increase of the scattering length $\Delta l^*(t)/l^*(0)$. For $L > l_a$, the diffuse transmittance may be written as [23]

$$T(L) = \frac{10 l^*}{3 l_a} \exp(-L/l_a). \tag{3.5}$$

Expanding Eq. (3.5) to three terms and dividing by $T(0)$, we find an expression for the normalized change in the diffuse transmittance $\Delta T(t)/T(0)$ as a function of $\Delta l^*(t)/l^*(0)$ [16]:

$$\frac{\Delta T(t)}{T(0)} = \frac{1}{2}\left[\frac{L}{l_a} + 1\right]\left(\frac{\Delta l^*(t)}{l^*(0)}\right) + \frac{1}{8}\left[\frac{L^2}{l_a^2} - \frac{L}{l_a} - 1\right]\left(\frac{\Delta l^*(t)}{l^*(0)}\right)^2 + \frac{1}{48}\left[\frac{L^3}{l_a^3} - 6\frac{L^2}{l_a^2} + 3\frac{L}{l_a} + 3\right]\left(\frac{\Delta l^*(t)}{l^*(0)}\right)^3 + \cdots. \tag{3.6}$$

During the experiments, $\Delta l^*(t)/l^*(0)$ increases rapidly to 0.20 10 s after applying the field, then increases linearly to 0.24 at 150 s as shown in Fig. 2. Thus, l^* varies by less than approximately 2% during our autocorrelation measurements and does not change when the field is stepped to lower values; it does return immediately to $l^*(0)$ when the field is turned off. This suggests that structure dominates l^* and there is a minimal amount of structural change when the field is reduced for our dynamic measurements.

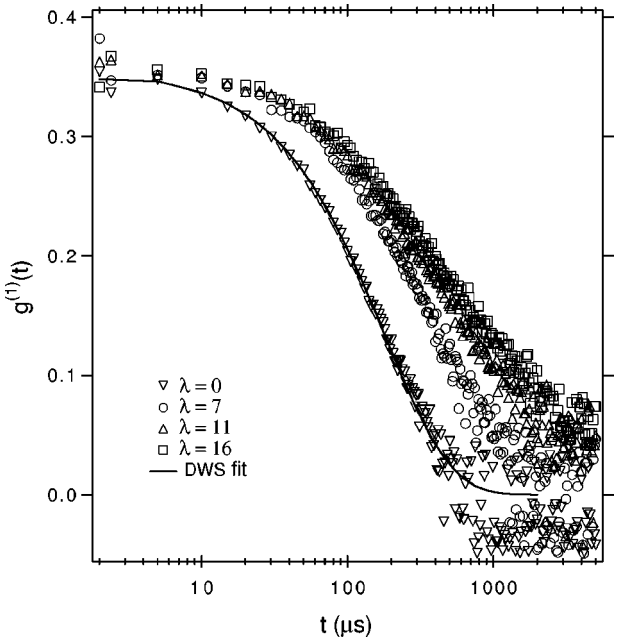

FIG. 3. Measured DWS autocorrelation functions for the isotropic MR suspension and three field strengths measured 90 s after applying the initial field. The solid line shows a fit of the solution to Eq. (3.1). Increasing λ shifts the decay to longer times.

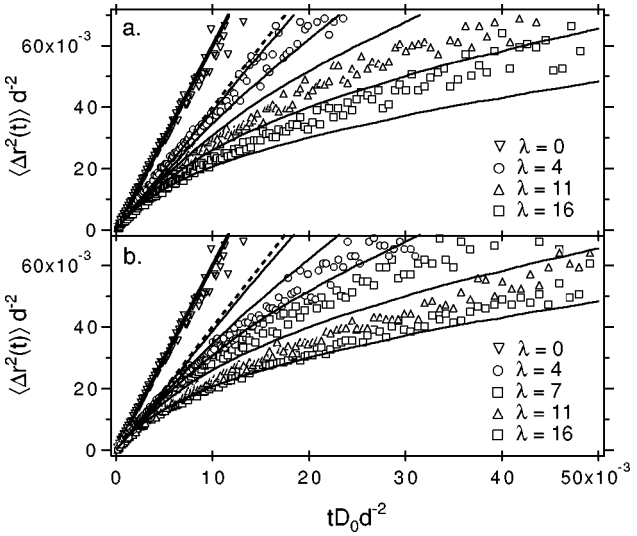

FIG. 4. $\langle \Delta r^2(t) \rangle$ calculated from $g^{(1)}(t)$ using the solution to Eq. (3.1). The straight, solid line represents 3D self-diffusion, the dashed line represents 2D self-diffusion, and the five curved solid lines are simulation results for dipolar chains of 100 particles with $\lambda = 5$, 10, 15, 20, and 26, increasing from left to right in the figures. (a) DWS data taken 15 s after applying the magnetic field. (b) Data taken 90 s after applying the field.

C. DWS results

As shown in Fig. 3, the autocorrelation $g^{(1)}(t)$ for the field-off data is well described by the isotropic solution of Eq. (3.1) by fitting l^* using our measured value for l_a and calculated value for D_s. The next three curves show $g^{(1)}(t)$ measured 90 s after applying the field. The autocorrelations now show a shift to longer decay times, increasing with higher values of λ. Unlike the isotropic case, the autocorrelations for the dipolar systems cannot be fit with a single characteristic decay time such as $(D_s k_0^2)^{-1}$. Instead, we calculate the mean-squared displacement with time $\langle \Delta r^2(t) \rangle$ from the solution of Eq. (3.1).

Figure 4 shows $\langle \Delta r^2(t) \rangle$ scaled by the particle diameter d for each dipole strength as a function of scaled time $tD_s d^{-2}$. The straight solid line in each plot represents self-diffusion, which the field-off data follows very well. When the field is applied, the initial mean-squared displacements follow a similar slope, which is less than that of free three-dimensional (3D) diffusion, but consistent with two-dimensional (2D) diffusion (the dashed, straight lines in Fig. 4) irrespective of dipole strength. As the time increases, $\langle \Delta r^2(t) \rangle$ diverges further from the free diffusion limit, exhibiting a constrained, subdiffusive motion. The magnitude of deviation from the solid line increases as we increase the dipole strength, suggesting that the DWS experiment is sensitive to the small-wavelength motions of the dipolar chains. The chains should exhibit a spectrum of modes of motion, including short-time individual ''vibrations'' of each particle, collective chain motion at intermediate timescales, and eventually the long-time diffusion of the entire chain. Since the scattering data for each field strength exhibits the same initial slope, our experiments appear to measure the Brownian motion of the particles comprising the dipolar chains. Particle diffusion is hindered by constraint to the chain through the dipolar interaction with its neighbors. Movement perpendicular to the chain direction dominates, indicated by the initial 2D motion, while the constraint increases as we increase the dipole strength, thereby stiffening the chains. It is also apparent that the mobility 90 s after applying the field is reduced further from the freely diffusing limit than that measured 15 s after applying the field, possibly due to the lateral aggregation of chains with time. This is consistent with the slow increase in l^* measured through the diffuse transmittance. Lateral aggregation should stiffen the magnetic chains further, and thus decrease chain segment motion.

D. Brownian dynamics simulations

To test our interpretation of the DWS experiments, we conduct Brownian dynamics simulations of magnetic chains over the time scales observed in our experiments [31,32]. Briefly, the simulations solve the equation of motion of the νth particle, taking into account four forces acting on it: a dipolar force between neighboring particles $F_i^{D,\nu}$, a stochastic Brownian force $F_i^{\mathrm{Br},\nu}$, Stokes drag $F_i^{S,\nu}$, and an excluded volume interaction $F_i^{\mathrm{EV},\nu}$. Again scaling displacement with the particle diameter d and time with the characteristic time a free particle diffuses its diameter $D_s d^{-2}$, the dimensionless equation of motion, neglecting inertia, is written in Einstein notation as

$$\dot{q}_i^{\nu} = \lambda F_i^{D,\nu} + F_i^{\mathrm{Br},\nu} + F_i^{S,\nu} + c F_i^{\mathrm{EV},\nu}, \tag{3.7}$$

where λ is the dipole strength. The simulations are conducted for $\lambda = 5$, 10, 15, 20, and 26 using ensembles of 500 chains for proper averaging. We compute the mean-squared deviation of each particle, $\langle \Delta r_\nu^2(t) \rangle$ averaged over all particles in the simulation for chains of 20 and 100 particles.

Since our experiments are most sensitive to lateral fluctuations in the chain, we extract the mean-squared displacement projected onto a plane orthogonal to the chain direction. We compare the 100 particle simulation results to the DWS data in Fig. 4. The differences in $\langle \Delta r_\nu^2(t) \rangle$ using 20 particles showed no consistent trend and did not exceed the expected accuracy. The simulations capture the qualitative aspects of the experimental results nicely; however, there are quantitative discrepancies for both the 15 and 90 s data. For instance, the simulations require a higher dipole strength to generate similar displacements with time. This could reflect the fact that the simulation neglects the local field created from the formation of the dipolar chains as well as higher moment interactions [6]. At this time we should not expect exact quantitative agreement for a variety of reasons including neglect of hydrodynamic interactions and magnetic interactions between chains.

IV. CONCLUSIONS

As a class of tunable fluids, MR systems are interesting due to their fast rheological response and possible applications in mechanical systems such as brakes and clutches. In this paper, we presented a study of the dynamics of nearly neutrally buoyant MR suspensions using diffusing-wave spectroscopy. By accounting for changes in the light transport properties of the system, we isolate variations in the chain dynamics caused by the interactions between the particles. The DWS experiments offer the capability to measure the dynamics of the MR fluid systems on time and length scales that capture the short-wavelength chain motions. Brownian dynamics simulations of dipolar chains support our experimental results. Both experiments and simulations show initial particle displacements that are independent of field strength; however, at longer times, we see a constrained sub-diffusive movement that increases with the dipolar interactions. We plan to investigate the quantitative agreement between simulations and experiments by incorporating hydrodynamic interactions and chaining effects into our simulations in the near future.

ACKNOWLEDGMENTS

The authors thank Patrick Doyle for his aid with the simulations, Jerome Bibette for providing the ferrofluid, and Marc Fermigier for fruitful discussions. Support by NASA (Grant No. NAG3-1887-1) is gratefully acknowledged.

[1] Z. Shulman, R. Gorodkin, E. Korobko, and V. Gleb, J. Non-Newtonian Fluid Mech. **8**, 29 (1981).
[2] G. Helgesen *et al.*, Phys. Rev. Lett. **61**, 1736 (1988).
[3] Y. Grasselli, G. Bossis, and L. Lemaire, J. Phys. II **4**, 253 (1994).
[4] D. Wirtz and M. Fermigier, Phys. Rev. Lett. **72**, 2294 (1994).
[5] J. Liu *et al.*, Phys. Rev. Lett. **74**, 2828 (1995).
[6] H. Zhang and M. Widom, Phys. Rev. E **51**, 2099 (1995).
[7] J. D. Carlson and K. D. Weiss, Machine Design **1994**, 61.
[8] J. D. Carlson and K. D. Weiss, in *Proceedings of the 5th International Conference of Electro-Rheological, Magneto-Rheological Suspensions and Associated Technology, Sheffield, England, July 10–14, 1995*, edited by W. Bullough (World Scientific, Singapore, 1996).
[9] K. Zahn, J. M. Mèndez-Alcaraz, and G. Maret, Phys. Rev. Lett. **79**, 175 (1997).
[10] J. H. E. Promislow, A. P. Gast, and M. Fermigier, J. Chem. Phys. **102**, 5492 (1995).
[11] J. H. E. Promislow and A. P. Gast, Langmuir **12**, 4095 (1996).
[12] J. H. E. Promislow and A. P. Gast, Phys. Rev. E **56**, 642 (1997).
[13] M. Hagenbüchle and J. Liu, Appl. Opt. **36**, 7664 (1997).
[14] A. Silva, B. Bond, F. Plouraboué, and D. Wirtz, Phys. Rev. E **54**, 5502 (1997).
[15] T. Halsey and W. Toor, J. Stat. Phys. **61**, 1257 (1990).
[16] J. M. Ginder, Phys. Rev. E **47**, 3418 (1993).
[17] J. Bibette, J. Colloid Interface Sci. **147**, 474 (1991).
[18] A. Gast and C. Zukoski, Adv. Colloid Interface Sci. **30**, 153 (1989).
[19] D. Pine, D. Weitz, J. Zhu, and E. Herbolzheimer, J. Phys. (France) **51**, 2101 (1990).
[20] D. Pine, D. Weitz, P. Chaikin, and E. Herbolzheimer, Phys. Rev. Lett. **60**, 1134 (1988).
[21] S. Fraden and G. Maret, Phys. Rev. Lett. **65**, 512 (1990).
[22] D. A. Weitz and D. J. Pine, in *Dynamic Light Scattering*, edited by W. Brown (Oxford University Press, New York, 1993), pp. 652–720.
[23] A. Z. Genack, in *Scattering and Localization of Classical Waves in Random Media*, edited by P. Sheng (World Scientific, Singapore, 1990), pp. 207–311.
[24] H. S. Carslaw and J. C. Jaeger, *Conduction of Heat in Solids*, 2nd ed. (Clarendon Press, New York, 1986).
[25] F. C. MacKintosh and S. John, Phys. Rev. B **40**, 2383 (1989).
[26] M. H. Kao, K. A. Jester, A. G. Yodh, and P. Collings, Phys. Rev. Lett. **77**, 2233 (1996).
[27] A. Heiderich, R. Maynard, and B. van Tiggelen, J. Phys. II **7**, 765 (1997).
[28] H. Stark and T. C. Lubensky, Phys. Rev. E **55**, 514 (1997).
[29] H. Stark *et al.*, J. Opt. Soc. Am. A **14**, 156 (1997).
[30] G. Maret, Curr. Opin. Colloid Interface Sci. **2**, 251 (1997).
[31] P. S. Doyle, Ph.D. thesis, Stanford University, 1997.
[32] H. C. Öttinger, *Stochastic Processes in Polymeric Fluids* (Springer, New York, 1996).